JOURNAL OF GEOPHYSICAL RESEARCH: ATMOSPHERES, VOL. 118, 85–100, doi:10.1029/2012JD018697, 2013

Precipitation in the Hindu-Kush Karakoram Himalaya: Observations and future scenarios

E. Palazzi,[1] J. von Hardenberg,[1] and A. Provenzale[1]

Received 21 August 2012; revised 20 November 2012; accepted 29 November 2012; published 16 January 2013.

[1] We study the properties of precipitation in the Hindu-Kush Karakoram Himalaya (HKKH) region using currently available data sets. We consider satellite rainfall estimates (Tropical Rainfall Measuring Mission), reanalyses (ERA-Interim), gridded in situ rain gauge data (Asian Precipitation Highly Resolved Observational Data Integration Towards Evaluation of Water Resources, Climate Research Unit, and Global Precipitation Climatology Centre), and a merged satellite and rain gauge climatology (Global Precipitation Climatology Project). The data are compared with simulation results from the global climate model EC-Earth. All data sets, despite having different resolutions, coherently reproduce the mean annual cycle of precipitation in the western and eastern stretches of the HKKH. While for the Himalaya only a strong summer precipitation signal is present, associated with the monsoon, the data indicate that the Hindu-Kush Karakoram, which is exposed to midlatitude "western weather patterns", receives water inputs in winter. Time series of seasonal precipitation confirm that the various data sets provide a consistent measurement of interannual variability for the HKKH. The longest observational data sets indicate a statistically significant decreasing trend in Himalaya during summer. None of the data sets gives statistically significant precipitation trends in Hindu-Kush Karakoram during winter. Precipitation data from EC-Earth are in good agreement with the climatology of the observations (rainfall distribution and seasonality). The evolution of precipitation under two different future scenarios (RCP 4.5 and RCP 8.5) reveals an increasing trend over the Himalaya during summer, associated with an increase in wet extremes and daily intensity and a decrease in the number of rainy days. Unlike the observations, the model shows an increasing precipitation trend also in the period 1950–2009, possibly as a result of the poor representation of aerosols in this type of GCMs.

Citation: Palazzi, E., J. von Hardenberg, and A. Provenzale (2013), Precipitation in the Hindu-Kush Karakoram Himalaya: Observations and future scenarios, *J. Geophys. Res. Atmos.*, *118*, 85–100, doi: 10.1029/2012JD018697.

1. Introduction

[2] The Hindu-Kush Karakoram Himalaya (HKKH) is the largest mountain region in the world, encompassing parts of or the entire countries of Afghanistan, Bangladesh, Bhutan, China, India, Nepal, Myanmar, and Pakistan. The HKKH region feeds some of the major rivers in Southeast Asia (such as the Ganges, the Brahmaputra, the Indus, the Yellow River, and the Yang-Tze), which bring water to more than 1.5 billion people.

[3] The position and characteristics of various orographic reliefs in the HKKH are major climatic drivers; the confluence of different mountain ranges makes the topography of this area so complex that the relationship between rainfall and topography still remains poorly defined.

[4] Estimating current precipitation, both rainfall and snowfall, in this region and its possible changes in the coming decades is thus a major challenge from both a scientific and geopolitical viewpoint, and a necessary step to develop appropriate adaptation strategies.

[5] Unique interactions among the atmosphere, cryosphere, and hydrosphere, and influences from multiple climatic systems, prevent treating the HKKH as a single region. In fact, the Hindu-Kush Karakoram (HKK) in the west and the Himalaya in the east, differ in circulation patterns and, by consequence, in sources and types of precipitation. The eastern Himalaya is mostly affected by monsoon-controlled dynamics: precipitation occurs during summer, owing to the moisture advected northward from the Indian Ocean by the southwest Indian monsoon [e.g., *Li and Yanali*, 1996; *Wu and Zhang*, 1998; *Krishnamurti and Kishtawal*, 2000]. In the HKK, precipitation occurs also during winter, mostly due to the influence of westerly winds bringing moisture from the Mediterranean and Caspian Sea [*Singh et al.*, 1995; *Archer*, 2001; *Archer and Fowler*, 2004; *Treydte et al.*, 2006; *Syed et al.*, 2006]. Different circulation patterns and precipitation regimes in the HKK and the Himalaya lead to different glacier dynamics

[1]Institute of Atmospheric Sciences and Climate, National Research Council (ISAC-CNR), Turin, Italy.

Corresponding author: E. Palazzi. Institute of Atmospheric Sciences and Climate, National Research Council (ISAC-CNR), Turin, Italy. (e.palazzi@isac.cnr.it)

2169-897X/13/2012JD018697

in the two regions. Many observational and model studies have highlighted that the total eastern Himalayan glacier mass balance has been distinctly negative in the last decades [*Solomon et al*., 2007], mainly due to significant regional warming. By contrast, relatively recent studies have indicated that some glaciers in the central Karakoram have thickened or been stable [*Schmidt and Nusser*, 2009]. The Baltoro glacier, located in the northern Pakistan and running through part of the Karakoram mountain range, has shown small and limited variations in its extension in the last 50 years [*Mayer et al*., 2006], possibly owing to the role of debris-covered areas in reducing ice ablation [*Scherler et al*., 2011]. Many other glaciers in the Karakoram range show stable conditions or even a slight mass gain [*Hewitt*, 2005; *Gardelle et al*., 2012], and recent estimates indicate a tendency to increasing snow cover in this area [*Tahir et al*., 2011]. Some of these changes have been suggested to be linked to an increasing trend of winter precipitation in the Karakoram [*Archer and Fowler*, 2004] as well as to a decreasing trend of summer temperatures [*Archer and Fowler*, 2006]. However, a clear understanding of why the Karakoram cryosphere behaves so differently from eastern Himalayan glaciers is still lacking.

[6] Understanding these and other changes (or the lack thereof) in the hydrological cycle requires the availability of high-resolution and high-quality precipitation data, but the complex orography of the region poses a serious obstacle to monitoring its hydrometeorology and microclimates, especially by in situ stations. In spite of the recent growing observational efforts in the HKKH, especially in the eastern Himalaya, the existing number of climate and meteorological stations is still low and the data provided by the existing network are largely biased by altitude, because most of the stations are located in valley floors, much lower in altitude than the zones of maximum precipitation, while very few are on mountain slopes and tops [*Archer and Fowler*, 2006]. Regions above 5 km still remain largely unexplored, mainly for technical reasons [*Winiger et al*., 2005], and high-altitude snowfall is poorly measured (see for example *Rasmussen et al*. [2012]).

[7] Given the importance of the hydrological cycle in this area, the aim of this paper is to analyze and compare rainfall patterns, seasonality, and trends in the HKK and Himalaya, making use of a wide ensemble of currently available data quantitatively assessing the current and expected changes of precipitation in HKKH.

[8] Several studies already quantified the reliability of individual precipitation data sets in the East Asian region. *Sohn et al*. [2011] used merged rain gauge and satellite precipitation data sets together with reanalysis products to evaluate the reliability of the Climate Anomaly Monitoring System-Outgoing Longwave Radiation Precipitation Index data for the purpose of monitoring large-scale precipitation variability in East Asia. *Yatagai and Kawamoto* [2009] estimated quantitatively orographic precipitation over the Himalayas using the Tropical Rainfall Measuring Mission (TRMM) satellite data acquired by the Precipitation Radar (PR) instrument. They validated the precipitation patterns seen by the TRMM/PR using the daily precipitation data provided by a dense network of rain gauges developed in the framework of the APHRODITE (Asian Precipitation Highly Resolved Observational Data Integration Towards Evaluation of Water Resources) project. *Bookhagen and Burbank* [2006] used rainfall data derived from the TRMM Precipitation Radar and Microwave Imager instruments (TRMM/PR and TRMM/TMI) for the time period 1998–2005 and found clear relationships between topographic characteristics of the Himalayan arc and rainfall location and amount. According to their study, rainfall maxima occur in the frontal regions along the entire Himalaya at an average elevation of 0.95 km (mean relief of 1.2 km), while the central Himalaya is characterized by an inner rainfall belt occurring at an average elevation of 2.1 km (mean relief of 2 km). The eastern and northwestern regions do not show this inner rainfall belt. *Krishnamurti et al*. [2009] used a modified version of the TRMM 3B42 algorithm and of the data of nearly 2100 APHRODITE rain gauges over India to apply a simple linear regression-based downscaling of the Florida State University multimodel superensemble, to provide improved forecasts of rain over India. *New et al*. [2001] presented a review of the existing precipitation data sets and analyzed the information about precipitation trends and variability on a global perspective. *Andermann et al*. [2011] made a comparative analysis of various gridded precipitation data sets, including remote sensing and interpolated rain gauge data, as well as ground-based precipitation measurements along the Himalayan front, giving an overview on the applicability for that region of precipitation data sets especially in the zones where relief has a pronounced impact on precipitation.

[9] In the present study, we compare satellite observations (TRMM 3B42), rainfall archives based on the interpolation on regular spatial grids of sparse in situ stations data (APHRODITE, Global Precipitation Climatology Centre (GPCC), and Climate Research Unit (CRU) data sets), merged satellite and rain gauge data (Global Precipitation Climatology Project (GPCP) climatology), reanalyses (ERA-Interim), and the precipitation provided by an ensemble of simulations of the state-of-the-art global climate model EC-Earth [*Hazeleger et al*., 2012]. We focus separately on the HKK and Himalayan subregions and verify how the various data sets represent the properties of precipitation in the two regions in terms of precipitation amounts, seasonality, and trends. We do not try to define a ground "truth" or a reference data set, but we highlight the biases between the various products, their similarities and discrepancies. The statistics of the climate model output in the historical period are compared to the climatology provided by the other data sets to assess the extent to which this global climate model reproduces the observed seasonality and long-term behavior of precipitation in the two focus regions. Future projections of precipitation trends in terms of rainfall averages and intensity are obtained with two scenarios produced by the model for the twenty-first century, based on the representative concentration pathways "RCP 4.5" and "RCP 8.5" [*Moss et al*., 2010].

[10] The paper is structured as follows. Section 2 presents the study areas, describes the rainfall data sets and the EC-Earth model. Section 3 provides a comparison of all data sets in terms of precipitation distribution over the HKKH and surrounding regions and analyses seasonality and trends in the HKK and Himalaya, during summer and winter. Section 4 discusses future precipitation projections under two different climate change scenarios. The implications of our findings and perspectives for future work are discussed in the conclusive section.

2. Study Areas and Precipitation Data Sets

2.1. Study Areas and Methodology

[11] The complex topography, circulation patterns, and climatic responses in different parts of the Hindu-Kush Karakoram Himalaya range make a global description of these mountain areas scarcely useful and suggest a division into subregions. In this work, we consider separately two main areas, the HKK in the west and the Himalaya in the east, which are exposed to different circulations, precipitation patterns and are characterized by different glacier behavior [*Bookhagen and Burbank*, 2010].

[12] We have defined two domains, shown in Figure 1, which contain the main subregions of the HKK and Himalaya mentioned above, in the ranges 71°E–78°E/32°N–37°N and 78°E–93°E/25°N–32°N, respectively. In the following, we analyze the seasonal cycle and long-term trends of summer and winter precipitation in the two domains, focusing on mountain areas with elevation higher than 1000 m. To this end, we use several observational data sets, reanalyses and outputs from the EC-Earth model. Throughout the paper, we define summer to include the months from June to September (JJAS), over which the summer monsoon typically manifests itself over the eastern stretches of the HKKH. Winter includes the months from December to April (DJFMA), due to the duration of the wintertime precipitation in this area, as discussed in detail below.

2.2. Observations and Reanalyses

[13] Although some individual, high-quality, monitoring stations have been installed in recent years, the observational effort provided by in situ station data in this area remains extremely uneven and nonhomogeneous. The sparse rain gauge network covers mainly valleys and lowland areas, leading to a bias toward the lower elevations in the observations. There are far more in situ stations measuring the standard meteorological parameters and the atmospheric composition in the eastern Himalaya than in the HKK, despite an increased effort in the Karakoram region in recent years. For example, the Nepal Climate Observatory at Pyramid (NCO-P, 27.95°N, 86.82°E), installed at 5079 m above sea level near the base camp area of Mt. Everest (eastern Nepal Himalaya), in the framework of the ABC-UNEP and SHARE-Ev-K2-CNR projects, is probably the most outstanding example of a high-altitude monitoring station performing continuous observations (since March 2006) of the microclimate, meteorology and atmospheric composition in the high Himalayas [*Bonasoni et al.*, 2010].

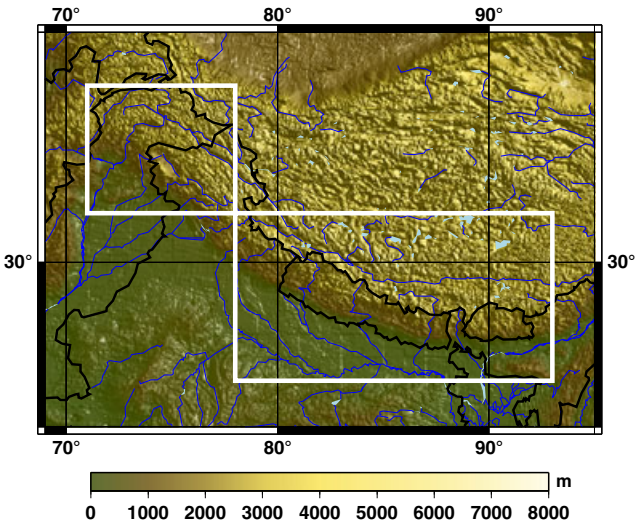

Figure 1. Map of the study area and the HKK (West) and Himalaya (East) domains.

[14] There have been several initiatives to collate the available, although sparse, historical rain gauge measurements and create gridded archives with the highest possible spatial resolution, in order to quantitatively represent the spatial distribution of precipitation.

[15] Gridding, based on different interpolation techniques, is a necessary step that reduces biases arising from the irregular station distribution and it is essential for the analysis of, e.g., regional precipitation trends. A great advantage of rain-gauge-based data sets is their long temporal coverage, extending back to the early decades of the 20th century. One of the major limitations of these data sets is the poor spatial coverage and high sparseness, especially in mountain regions, which constitutes a potential source of uncertainty when interpolating grid point values from the nearest few available stations. For short averaging time scales the spatial intermittency of precipitation represents a major source of uncertainty for these approaches. On the other hand, remote sensing techniques, especially satellite-based, can provide spatially-complete coverage of precipitation estimates, but they do not extend back beyond the 1970s and as such are not yet suitable for assessing long-term trends and performing climatological studies. The shortcomings of satellite data and of surface station data have stimulated the development of combined satellite rain gauge data sets, in order to maximize the benefits and minimize the disadvantages of the two approaches.

[16] It is important to recall that both in situ station data and satellite estimates, and their combinations, have difficulties in detecting the snow component of precipitation [*Rasmussen et al.*, 2012]. This is due to a wide range of issues, ranging from the scarcity of high-elevation in situ stations, to the interference of wind with the sensors and to problems of satellite-based meteorological radars in identifying snow crystals. A fourth possibility for precipitation analysis at global and regional scales is to make use of reanalysis systems, which use data assimilation techniques to keep the output of a numerical global circulation model close to observations. Contrary to most observations, reanalysis data do account for total precipitation (rainfall plus snow). It is worth pointing out that climate trends obtained from reanalysis data should be regarded with caution, since continuous changes in the observing systems and biases in both observations and models can introduce spurious variability and trends into reanalysis output [e.g., *Bengtsson et al.*, 2004].

[17] Three interpolated data sets (APHRODITE, GPCC, and CRU), the TRMM 3B42 satellite product based on the merging of different remote-sensing and ground-control data, the GPCP combined precipitation data set, and the ERA-Interim reanalyses, all employed in the present study, are briefly described below.

(1) Asian Precipitation Highly-Resolved Observational Data Integration Towards Evaluation of Water Resources: This project, conducted by the Research Institute for Humanity and Nature and the Meteorological Research Institute of the Japan Meteorological Agency since 2006, develops state-of-the-art daily precipitation data sets with relatively high spatial resolution grids (0.25°, 0.5°) for Asia (see http://www.chikyu.ac.jp/precip/products/index.html). Details on the gridding procedure and on the reliability of daily interpolated precipitation fields can be found in *Yatagai et al*. [2009, 2012]. For the present study, we have used the Monsoon Asia (60°E–150°E longitude, 15°S–55°N latitude) domain of APHRODITE. The data set version employed here (APHRO_V1003R1), which does not include a discrimination between rain and snow, is characterized by a spatial resolution of 0.25° latitude-longitude, extending from 1951 to 2007.

(2) Climate Research Unit: The most recent version (July 2012) of the CRU TS 3.1 data set (CRU TS 3.01.01) from the University of East Anglia has been used, consisting of monthly gridded fields of precipitation over land areas (excluding Antarctica), based on daily values, from 1901 to 2009 with a spatial resolution of 0.5° latitude-longitude. CRU TS 3.1 data are produced using the same methodology as for the previous 3.0 version [*Mitchell and Jones*, 2005]. The main differences is that the 3.1 data set extends from 1901 to 2009. The recent data set used here includes the correction of a systematic error in precipitation which has been detected in July 2012.

(3) Global Precipitation Climatology Centre: Established in 1989 on request of the World Meteorological Organization, GPCC is operated by the Deutscher Wetterdienst (National Meteorological Service of Germany) in the framework of the World Climate Research Program. The GPCC data set consists of global analyses of monthly precipitation data on the Earth's land surface, based on in situ rain gauge data, at the 0.5° latitude-longitude resolution from 1901 to 2009. In this study, we have used the GPCC v5 product.

(4) Global Precipitation Climatology Project: GPCP is an element of the Global Energy and Water Cycle Experiment, established by the World Climate Research Program in 1986 with the initial goal of providing monthly mean precipitation data on a 2.5° grid. We have used the latest available version (v2.2) of monthly means of precipitation derived from a combination of precipitation estimates from low-orbit satellite microwave data, geosynchronous-orbit satellite infrared data, and surface rain gauge observations, from 1979 to 2010 [*Adler et al*., 2003]. GPCC and GPCP are linked in that, from 1986 to the present, GPCC monthly rain gauge analyses constitute the in situ component of the GPCP data set.

(5) ERA-Interim reanalyses: ERA-Interim is the latest global atmospheric reanalysis produced by the European Centre for Medium-Range Weather Forecasts, covering the period from 1979 onwards. Estimates of precipitation associated with the reanalysis are produced by the forecast model, based on temperature and humidity information derived from assimilated observations. Precipitation is not assimilated in the model. These data are available at a daily resolution on a 0.75° latitude-longitude grid.

(6) TRMM 3B42 data: We have analyzed 13 years (1998–2010) of the TRMM 3B42 (version 6) product [*Huffman et al*., 2007], available through the NASA Mirador interface (http://mirador.gsfc.nasa.gov). TRMM 3B42 is a precipitation data set that combines data from several passive microwave radiometers and infrared observations, then corrected with the monthly field ratios between the TRMM 3B43 product (monthly version of TRMM 3B42) and gauge stations. TRMM 3B42 data have a 0.25° spatial and 3 h temporal resolution, and are available on a global belt extending, approximately, from 50°S to 50°N latitude. Technical details and the description of the algorithm 3B42 can be found at http://trmm.gsfc.nasa.gov/3b42.html. *Kamal-Heikman et al*. [2007] reported an underestimation of precipitation amounts provided by this product in mountainous regions particularly affected by snowfall contribution.

[18] Table 1 summarizes the main characteristics, such as the temporal and spatial sampling and resolution of the six precipitation data sets employed in this study.

2.3. The EC-Earth Global Climate Model

[19] Precipitation estimates from the EC-Earth GCM were included in the analysis, with a threefold aim: (1) Supplying a further "instrument" giving precipitation estimates in the two focus regions; (2) evaluate the extent to which a global climate model can reproduce precipitation patterns, seasonality, and long-term behavior of precipitation in a limited area, though having a coarse resolution, and (3) evaluate future scenarios and possible trends in the HKK and Himalaya under different forcing conditions. EC-Earth is a state-of-the-art

Table 1. Main Characteristics of the Observational and Reanalysis Precipitation Data Sets Analyzed

Data Set	Product	Spatial Domain	Temporal Domain	Spatial Resolution	Temporal Resolution
TRMM	3B42	Tropics (50°S–50°N)	1998–2010	0.25° lat-lon	3 hourly
GPCP	V2.2	Global 1.25°E–358.75°E 88.75°S–88.75°N	1979–2010	2.5° lat-lon	Monthly
APHRODITE	APHRO_V1003R1 Monsoon Asia	Land 60°E–150°E 15°S–55°N	1951–2007	0.25° lat-lon	Daily
GPCC	V5	Land	1901–2009	0.5° lat-lon	Monthly
CRU	CRU TS 3.01.01	Land	1901–2009	0.5° lat-lon	Monthly
ERA-Interim	Reanalyses	Global	1979–2011	0.75° lat-lon	Daily

Earth System Model, based on the concept of seamless prediction [*Hazeleger et al*., 2012] developed in the framework of the European Consortium EC-Earth, which includes more than 20 research institutions, universities and other public parties from ten different countries. The core of the EC-Earth model is a fully coupled atmosphere-ocean-sea ice model system joining the Integrated Forecast System of the European Centre for Medium-Range Weather Forecasts and the ocean model Nucleus for European Modelling of the Ocean (NEMO) [*Madec*, 2008]. It also includes the land surface modulus H-Tessel [*Dutra et al*., 2010] and the sea-ice model LIM-2 [*Fichefet and Morales-Maqueda*, 1997]. The standard EC-Earth (v2.3) configuration runs at T159 horizontal spectral resolution (corresponding to about 1.125° grid resolution) with 62 vertical levels, for the atmosphere, and an irregular grid with about 1 degree resolution and 42 vertical levels for the ocean.

[20] For this work we used the EC-Earth model to simulate climate in the period 1850–2005, using reconstructed historical anthropogenic forcing and solar variability (according to CMIP5 prescriptions), and to create two scenarios for the period 2006–2100, based on the two representative concentration pathways (RCPs) for anthropogenic emissions RCP 4.5 and RCP 8.5 [*Moss et al*., 2010]. RCP 4.5 [*Thomson et al*., 2011] is a scenario that stabilizes anthropogenic radiative forcing at 4.5 W m^{-2} (compared to preindustrial) in the year 2100. The more extreme RCP 8.5 scenario [*Riahi et al*., 2011] assumes no effective climate change policies and a continuation of high energy demand and high greenhouse gas emissions, leading to 8.5 W m^{-2} of anthropogenic radiative forcing in 2100.

3. Precipitation Climatology

3.1. Rainfall Distribution Over the HKKH Region

[21] The spatial distribution of summer (JJAS) and winter (DJFMA) precipitation over a region that includes the HKKH range obtained from the APHRODITE, CRU, GPCC, TRMM, GPCP, and ERA-Interim data sets and from EC-Earth, is shown in Figures 2 and 3, respectively. Precipitation is averaged over the period 1998–2007 for which data from all six archives are available. Precipitation data from EC-Earth have been averaged over the same decade, through an extension of the historical run ending in December 2005 using the RCP 4.5 scenario data. Please note that the color scales in Figures 2 and 3 are not the same for summer and winter precipitation.

[22] All data sets coherently reproduce the key features of summer and winter precipitation in the HKKH region. During summer (Figure 2), precipitation is concentrated over the eastern stretch of the Himalaya and decreases from southeast to northwest along the Himalayan chain. Mountain regions in northern Pakistan are quite dry during summer, reaching a maximum precipitation of about 3–4 mm d^{-1}. During winter (Figure 3), while the whole Himalayas receive considerably lower precipitation amounts than during summer, the land masses of northern Pakistan receive a water input carried by eastward propagating midlatitude patterns. Moisture-laden westerly winds are intercepted as they encounter high mountain ranges in northern Pakistan, leading to moisture condensation and precipitation at high altitudes and dry conditions at the interior high plains.

[23] Although the key features of the precipitation field over the target area are well represented by all data sets, important discrepancies arise from the different temporal and spatial sampling and resolution and from the specific characteristics of the various products, such as different bias correction, homogenization or interpolation choices. Important differences are observed in winter precipitation over North Pakistan and in summer precipitation over Nepal, two periods which are essential for the hydrologic budget of these two areas. It is also important to point out that while the reanalysis and global climate model data estimate the total precipitation (including snow), the APHRODITE, CRU, and GPCC station data and the TRMM 3B42 product provide rainfall estimates.

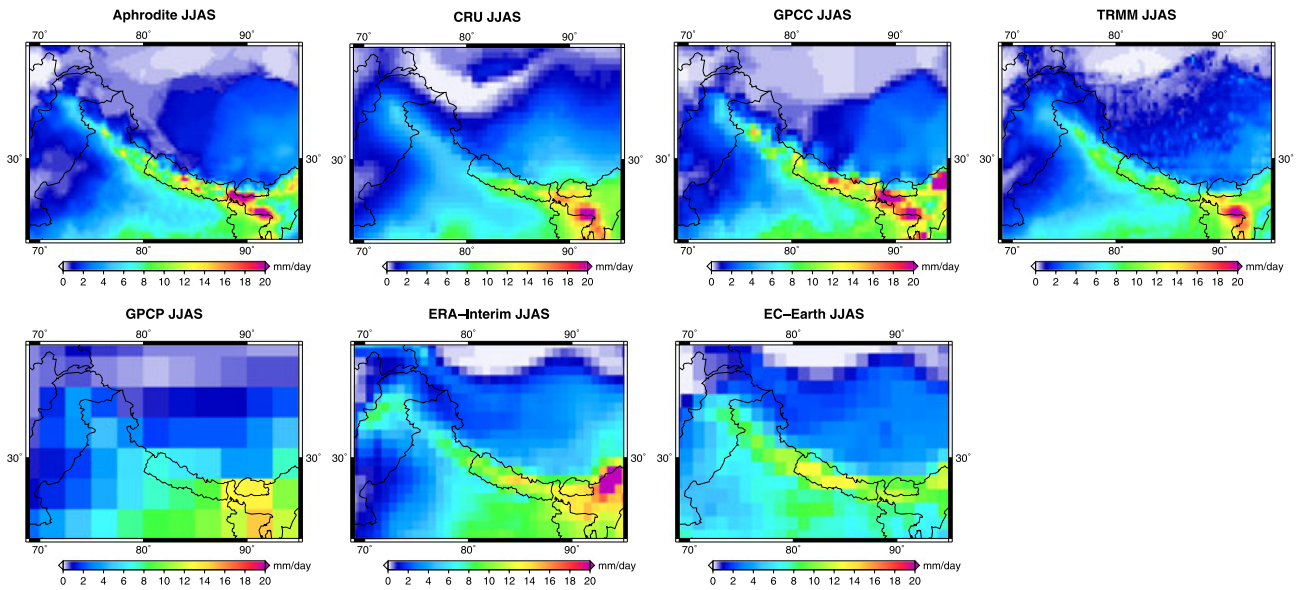

Figure 2. Multiannual mean (1998–2007) of summer (JJAS) precipitation over the region between 69°E–95°E and 23°N–39°N from the APHRODITE, CRU, GPCC, TRMM, GPCP, ERA-Interim, and EC-Earth model data sets.

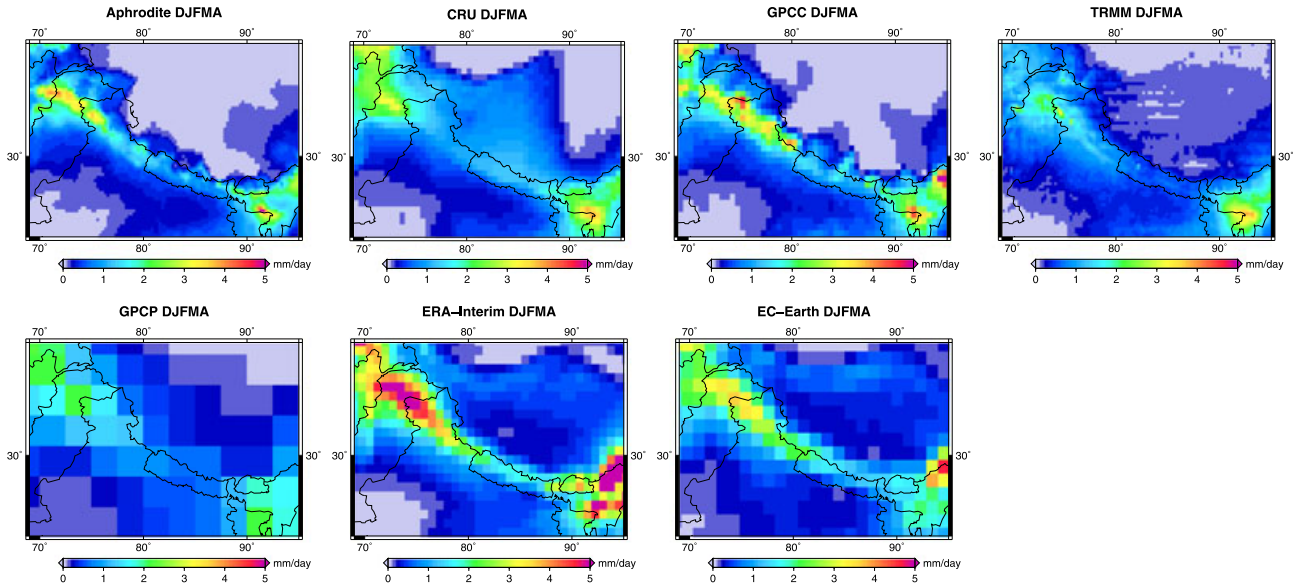

Figure 3. Same as Figure 2 for winter (DJFMA).

[24] In areas with sparse station coverage, the GPCC, APHRODITE, and CRU data sets interpolate grid-point values from the nearest few available stations, introducing a significant element of uncertainty. An example of the application of the interpolation procedure to the GPCC archive is given in Figure 4 illustrating the transition from sparse in situ station data to the final gridded product. Another example is given in Figure 5 showing, for the APHRODITE data set, the multiannual mean summer distribution over the HKKH and surrounding areas of precipitation (right panel) and of the RSTN index (left panel), defined as the ratio of valid station grids in the 0.25° analysis, giving a measure of the reliability of the daily interpolated precipitation fields in the APHRODITE final product [*Yatagai et al.*, 2009, 2012].

3.2. Seasonal Cycle

[25] Because we focus on the behavior of precipitation in high-elevation regions in HKKH, in all the following analyses we consider only the data and model outputs from pixels/grid points with mean elevation higher than 1000 m above mean sea level. The annual cycle of precipitation averaged over the high-elevation regions of the HKK domain (solid lines) and from of the Himalaya domain (dashed lines) from the APHRODITE, CRU, GPCC, TRMM, GPCP, ERA-Interim data sets, and from the EC-Earth model is reported in the left panel of Figure 6. The mean annual cycle of precipitation is calculated as the average over the time period 1998–2007 which is common to all data sets. All data sets give a similar picture of the monthly climatology of precipitation, with a bimodal distribution in the HKK and a unimodal distribution in the Himalaya. In fact, the figure is consistent with the two principal sources of precipitation in the whole HKKH range. The monsoon represents the dominant source in terms of total amounts of precipitation delivered, bringing storm systems from the south to the Himalayan range in the period from late June through September, with a maximum in July, coherently reproduced by all data sets. The precipitation peak in July is lower for APHRODITE and TRMM (around 5 mm d^{-1}) than

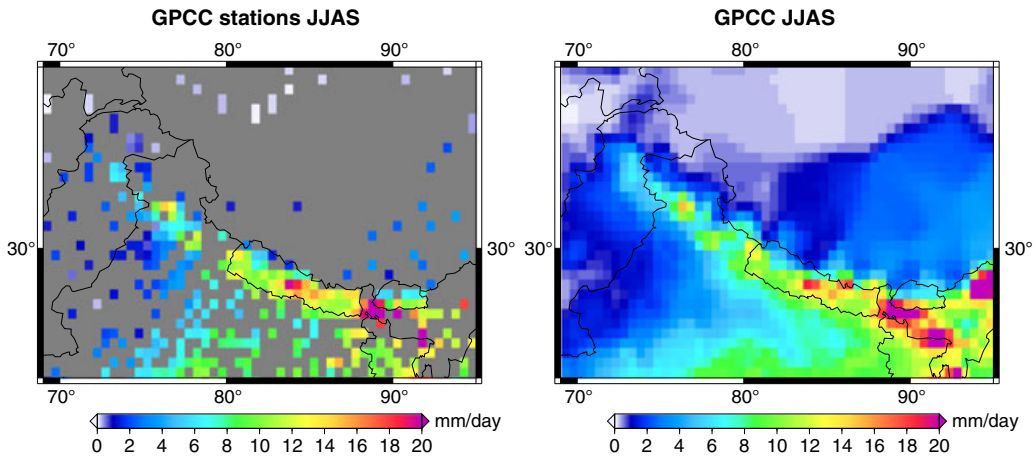

Figure 4. Multiannual mean (1998–2007) of summer (JJAS) precipitation over the HKKH and surrounding areas from GPCC: (left) the original station data and (right) the gridded data. The figure highlights the effect of the interpolation process.

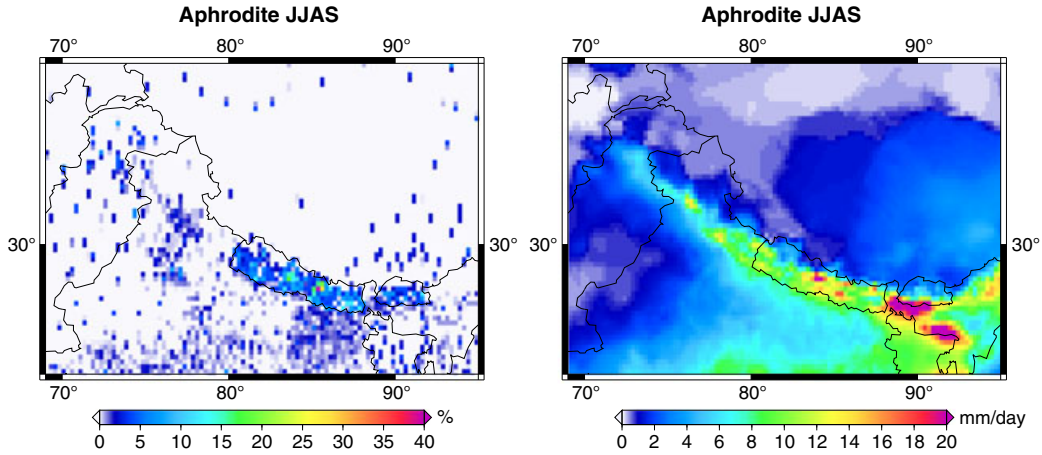

Figure 5. Multiannual mean (1998–2007) of summer (JJAS) RSTN index (left, see text) and precipitation (right) over the HKKH and surrounding areas from APHRODITE.

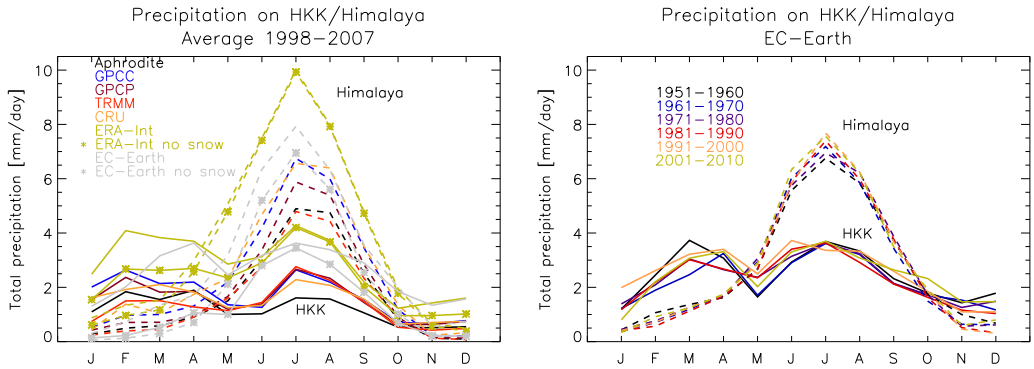

Figure 6. (left) Monthly climatology of precipitation (averaged over the period 1998–2007) for the HKK domain (solid lines) and the Himalaya domain (dashed lines), for the APHRODITE, GPCC, GPCP, TRMM, CRU, ERA-Interim, and EC-Earth data sets. The lines marked with stars indicate liquid precipitation only (obtained subtracting the snowfall flux from total precipitation for ERA-Interim and EC-Earth). (right) Mean annual cycle of precipitation in the HKK domain (solid lines) and Himalaya domain (dashed lines) from the EC-Earth model, averaged over different model decades as indicated in the figure legend.

for GPCP (around 5.5-6 mm d^{-1}), CRU and GPCC (6.5 mm d^{-1}) and ERA-Interim (around 10 mm d^{-1}). In the HKK domain a further source of precipitation occurs in winter/early spring (February/April), which is known to be associated with midlatitude westerly weather systems.

[26] ERA-Interim overestimates precipitation compared to the other data sets. The wintertime peak, whose timing is anyway consistent with observations, is about 4 mm d^{-1}. Precipitation for EC-Earth in the Himalaya is in better agreement with the observations than ERA-Interim. In the HKK domain, EC-Earth precipitation is higher than the satellite/in situ derived observations, but still lower than ERA-Interim.

[27] As already mentioned, both in situ station data and satellite estimates have difficulties in detecting the snow component of precipitation. This could lead to an underestimation of precipitation, particularly in snow-rich areas such as the HKKH and especially in winter. Even if some of the observational, satellite and merged data sets considered here have been treated for bias correction, this issue may contribute to the higher precipitation values found for ERA-Interim and EC-Earth. To explore this point, we report in the left panel of Figure 6 the contribution of liquid-only precipitation for EC-Earth and ERA-Interim (lines with stars), obtained by removing the snowfall flux from the total precipitation. An improvement is indeed observed for ERA-Interim, which gets closer to the observations in winter in HKK. EC-Earth displays an overall lowering of precipitation amounts after removing snowfall. In the HKK domain in winter the liquid precipitation component becomes significantly lower than the observations. One possibility is that measured precipitation (especially from rain gauges) includes a partial contribution from snow (typically, snow underestimates are very variable and can easily reach a factor of 2 or more, see *Rasmussen et al.* [2012]). On the other hand, the model may overestimate snow with respect to rainfall, particularly during winter. It is indeed known that EC-Earth has, globally, a cold bias [*Hazeleger et al.*, 2012], which could cause a wrong partition between snow and rain, probably associated with a model overestimation of snow cover and surface albedo during winter and spring [*Dutra et al.*, 2011]. The EC-Earth temperature bias averaged over the elevated regions of the HKK in winter (also averaged over the time period 1998–2007), evaluated

against ERA-Interim, is ~–5.5°C, while the maximum and minimum cold bias values reached in the HKK domain during winter are, respectively, –8.6°C and –2.1°C. For completeness, we also report the mean, maximum, and minimum cold bias values in the Himalaya domain during winter (–3.2°C, –4.9°C, –0.7°C respectively) and during summer (–4.4°C, –6.7°C, –1.9°C, respectively), and in the HKK domain during summer (–0.78°C, –5°C, –2.3°C respectively).

[28] Thanks to the long time span covered by the EC-Earth runs, we can also explore the decadal variability of the seasonal signal. The right panel of Figure 6 shows multiannual averages of monthly precipitation from EC-Earth, averaged over different decades in the period from 1951 to 2010 (through the extension of the historical run using the data from the RCP 4.5 scenario). While this variability is in general small, compared to the average precipitation amplitudes, the strongest decadal variability is found in summer for the Himalaya and in winter for the HKK domain, consistent with the importance of different large-scale synoptic patterns in different seasons for these two regions.

3.3. Interannual Variability

[29] Time series of yearly average winter and summer precipitation for the two subregions are shown in Figure 7. Note the different vertical axes for different domains and seasons, which have been used to better highlight how the various products can capture the interannual variability of precipitation and to facilitate their comparison. Figure 7 indicates that the elevated regions of the HKK domain receive comparable amounts of precipitation during summer and winter, while in the Himalaya summer precipitation largely exceeds winter precipitation.

[30] The correlation coefficients between pairs of time series, computed using seasonal mean values, are reported in Tables 2 and 3 for HKK and Himalaya, respectively. Data below the diagonal refer to winter. The correlation values associated with each pair refer to overlapping time periods of different length, and, therefore, they have been calculated on different numbers of data points. For example, TRMM and APHRODITE overlap for only 10 years, while GPCC and CRU overlap for 109 years, APHRODITE and CRU for 57 years, and so on (see Table 1).

[31] APHRODITE has very high correlation values with GPCC and GPCP in both seasons, both for the Himalaya and for HKK. The extremely high correlations found between GPCC and GPCP, in both summer ($r > 0.85$) and winter ($r > 0.84$), could be expected because GPCC data are the in situ components of the GPCP data set. Interestingly, Figure 7 shows that despite being highly correlated, the GPCC and GPCP data sets do not always agree in terms of precipitation amounts in both domains. This could reflect the local effect of bias adjustments in the data sets. The CRU data generally present lower correlations in the Himalaya than in the HKK region, possibly due to a different coverage in terms of stations in the two areas.

[32] The correlations of TRMM measurements with all in situ based data sets are higher in winter than in summer (except with CRU). It is important to point out that some of these low correlations are probably due to the fact that most rain gauges are located in the valley bottom, while

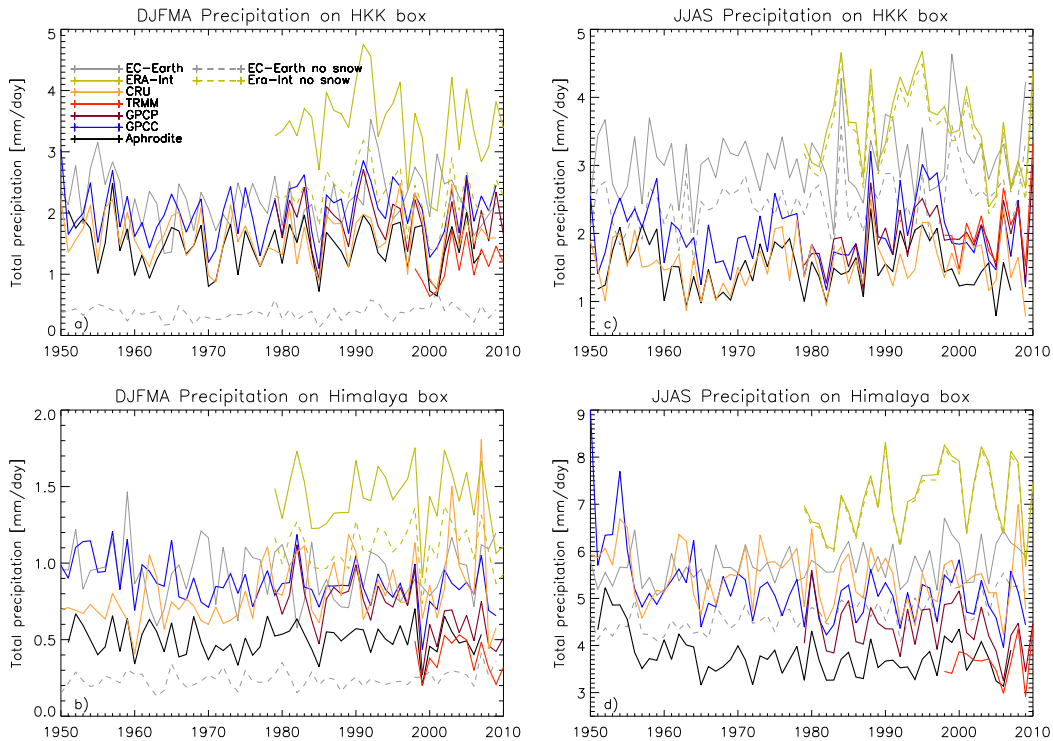

Figure 7. Time series of precipitation over (a,c) the HKK domain and (b,d) the Himalaya domain during DJFMA (Figures 7a and 7b) and JJAS (Figures 7c and 7d) for the APHRODITE, GPCC, GPCP, TRMM, CRU, and ERA-Interim data sets (from 1950 onwards), and from the EC-Earth model, shown as the grey line. The dashed lines are for liquid precipitation (that is, after removing snow), for ERA-Interim and for the EC-Earth model.

Table 2. Correlation Coefficients Between Pairs of Time Series for Precipitation During Summer and Winter in the HKK. Data Above (below) the Diagonal Refer to the Summer JJAS (Winter DJFMA) Period. The Overlapping Years for the Various Data Set Pairs are: 1998–2007 (APHRODITE-TRMM), 1998–2009 (CRU-TRMM, GPCC-TRMM), 1998–2010 (GPCP-TRMM, TRMM-ERA-Interim), 1979–2007 (APHRODITE-GPCP, APHRODITE-ERA-Interim), 1979–2009 (GPCC-GPCP, CRU-GPCP, GPCC-ERA-Interim, CRU-ERA-Interim), 1979–2010 (GPCP-ERA-Interim),1951-2007 (APHRODITE-GPCC, APHRODITE-CRU), 1901–2009 (CRU-GPCC)

HKK		JJAS					
		APHRODITE	CRU	GPCC	GPCP	TRMM	ERA-Interim
	APHRODITE	–	0.59	0.88	0.80	0.51	0.61
	CRU	0.79	–	0.71	0.77	0.79	0.51
DJFMA	GPCC	0.84	0.72	–	0.90	0.78	0.58
	GPCP	0.94	0.76	0.95	–	0.93	0.56
	TRMM	0.73	0.69	0.89	0.87	–	0.60
	ERA-Interim	0.80	0.75	0.78	0.81	0.83	–

Table 3. The Same as Table 2 for the Himalaya Domain

Himalaya		JJAS					
		APHRODITE	CRU	GPCC	GPCP	TRMM	ERA-Interim
	APHRODITE	–	0.69	0.88	0.86	0.48	0.59
	CRU	0.41	–	0.38	0.69	0.78	0.46
DJFMA	GPCC	0.76	0.23	–	0.85	0.51	0.69
	GPCP	0.84	0.48	0.84	–	0.55	0.48
	TRMM	0.84	0.62	0.85	0.80	–	0.49
	ERA-Interim	0.79	0.54	0.80	0.73	0.89	–

highest rainfall amounts occur near or at the mountain peaks and are usually much higher. It is exactly this signal that the remote sensing data are most sensitive to [*Bookhagen and Burbank*, 2006; *Barros et al*., 2000].

[33] ERA-Interim data have a generally good correlation with the main in situ and merged observational data sets during winter, while they correlate less in summer, particularly for the Himalaya. The precipitation of ERA-Interim has a significant high bias compared to the observational data sets.

[34] The fact that summer correlations are generally lower than winter correlations could be a symptom of difficulties, either of the satellite or the rain gauges or of the combined and reanalysis products, in consistently measuring precipitation during intense monsoonic episodes.

[35] The interannual fluctuations of EC-Earth precipitation, shown as the grey lines in Figure 7, cannot be correlated with observations, because the model runs in climate mode (while the model attempts to reproduce the properties of real climate in a statistical sense, there will be no exact agreement with observations in any particular year). For the HKK domain during summer we find a high bias of almost 1 mm d^{-1} compared to observations, similar to that observed for ERA-Interim. It is possible that this bias is of dynamical origin and linked with an excessive summer monsoonal flow, with associated precipitation, extending to this region, as discussed further below.

[36] As noted previously, some of the biases between EC-Earth or ERA-Interim and the observations may be linked to difficulties in measuring the snow component of precipitation. For completeness, we report the contribution of liquid-only precipitation for EC-Earth and ERA-Interim, shown with the dashed lines in Figure 7. The same considerations discussed above for seasonality apply also in this case.

3.4. Long-term Trends

[37] Table 4 summarizes the values of JJAS and DJFMA precipitation trends obtained from the various data sets for HKK and Himalaya. Note that the table also shows, for each data set, the period of time over which trend calculation is performed to emphasize that trends from the various sources

Table 4. Precipitation Trends (in mm d^{-1} yr^{-1}) in the HKK and Himalaya During Summer (JJAS) and Winter (DJFMA) for the Various Data Sets (in Parentheses the Years Over Which Trends Have Been Calculated). Bold Figures are Significant at the 95% Level (*p*-value Indicated in Brackets)

	JJAS		DJFMA	
	Himalaya	HKK	Himalaya	HKK
APHRODITE (1951–2007)	**–0.010(*p*=0.001)**	0.0	0.0	–0.003
CRU (1950–2009)	–0.008	0.002	**0.005(*p*=0.004)**	–0.001
GPCC (1950–2009)	**–0.021(*p*=0.001)**	0.0	**–0.004(*p*=0.000)**	0.002
TRMM (1998–2010)	0.015	0.057	–0.006	0.041
GPCP (1979–2010)	–0.012	**0.017(*p*=0.045)**	**–0.010(*p*=0.001)**	–0.007
ERA-Interim (1979–2010)	0.027	–0.011	–0.002	–0.012
EC-Earth (1950–2009)	**0.008(*p*=0.002)**	0.005	–0.001	0.0
* ERA-Interim (1979–2010)	0.027	–0.011	0.0	–0.007
* EC-Earth (1950–2009)	**0.014(*p*=0.000)**	**0.007(*p*=0.027)**	**0.001(*p*=0.050)**	0.001

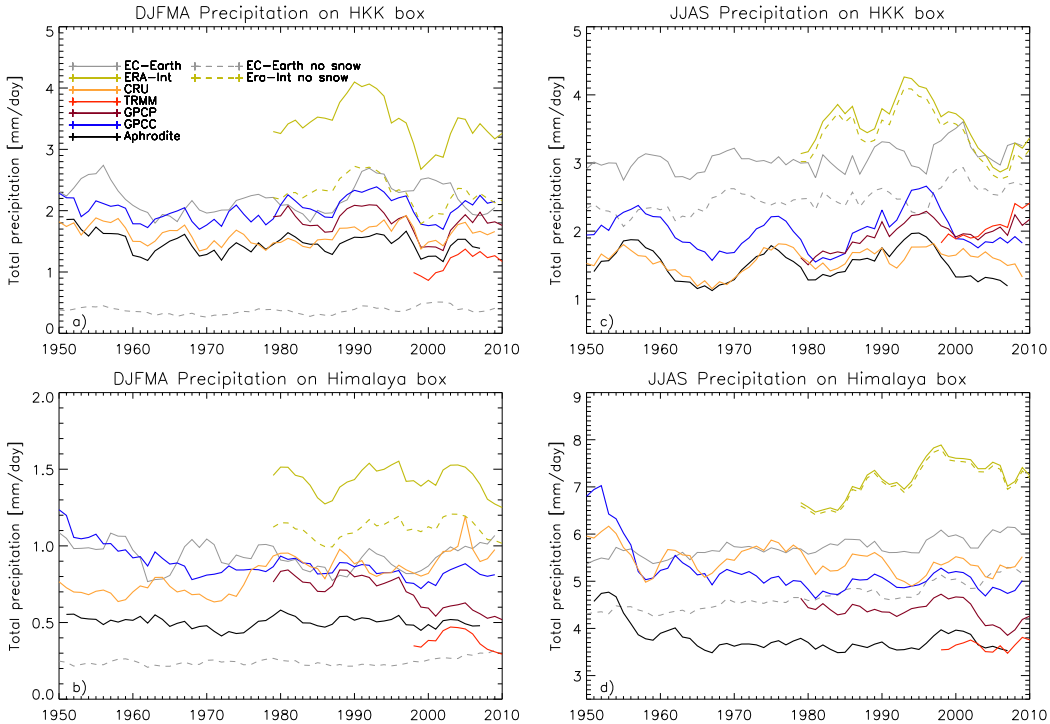

Figure 8. Same as Figure 7, after filtering the time series with a 5 years running mean.

refer to different periods. To help identify visually long-term variations, Figure 8 shows the precipitation time series after-application of a 5 year running mean. Starred entries in Table 4 indicate the ERA-Interim and EC-Earth liquid precipitation data. Data in bold style refer to trend values that are statistically significant at the 95% confidence level (the corresponding *p*-value is indicated in brackets). Statistical significance against the null-hypothesis of no trend has been determined using a Monte Carlo method based on randomly shuffling the series in time (1000 realizations were used) [*Ciccarelli et al.*, 2008]. For completeness, in Figure 9 we show the spatial pattern of JJAS precipitation trends in the target area, over the period of time indicated in Table 4 for the various data sets.

[38] None of the spatially averaged precipitation time series provides statistically significant evidence of long-term trends

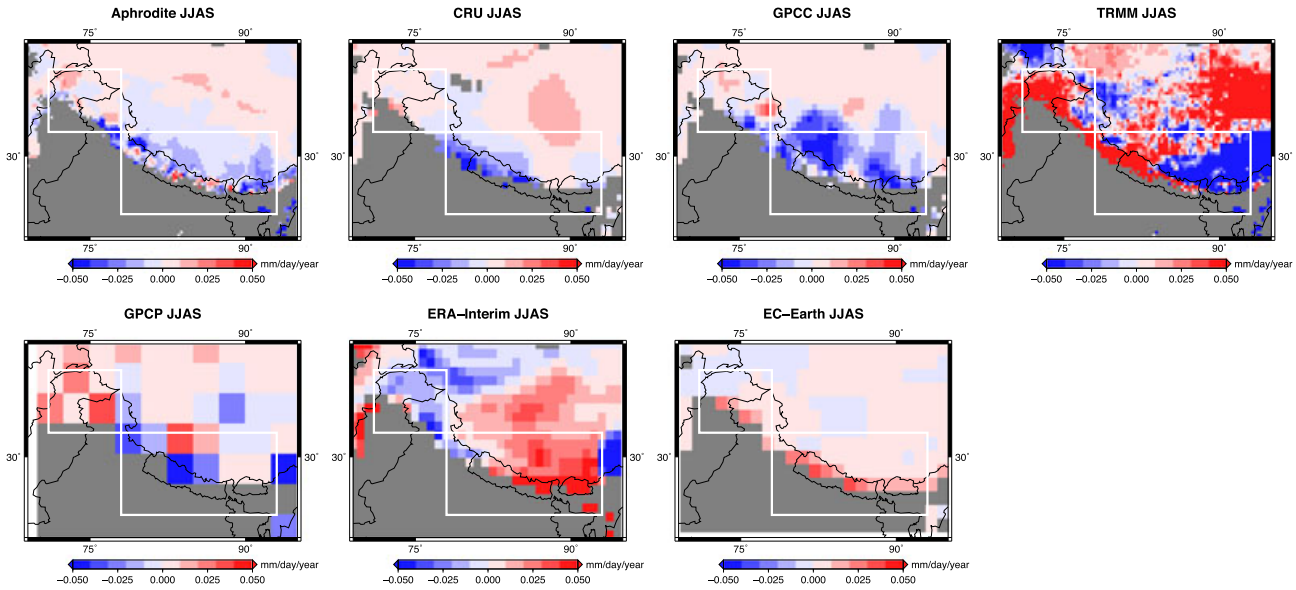

Figure 9. Spatial maps of summer (JJAS) precipitation trends for the APHRODITE, CRU, GPCC, TRMM, GPCP, ERA-Interim, and EC-Earth model data sets. Trends are computed over the same years as indicated in Table 4 and for areas above 1000 m in altitude. The boxes show the HKK (west) and Himalaya (east) regions over which average trends discussed in the text have been computed.

in HKK in winter. In HKK during summer, GPCP provides a statistically significant increasing trend of 0.017 mm d^{-1} yr^{-1} and so does EC-Earth (0.007 mm d^{-1} yr^{-1}). *Archer and Fowler* [2004] discussed seasonal precipitation trends in the Karakoram region and found an upward trend in winter precipitation in the period 1961–1999, statistically significant at three out of seventeen stations they analyzed (Skardu, 2210 m; Shahpur, 2012 m; Dir, 1425 m). It is interesting that no such trend emerges from the analysis of the ensemble of data sets considered here. Quite a different study was performed by *Treydte et al*. [2006] who presented a millennial-scale reconstruction of precipitation variability in the high mountains of northern Pakistan using an annually resolved oxygen isotope record from tree-rings. Their analysis revealed an increase of precipitation during the late 19th and the 20th centuries, yielding the wettest conditions of the past 1000 years, preceded by dry conditions at the beginning of the past millennium and through the eighteenth and early nineteenth centuries.

[39] In the Himalaya during winter, the CRU data indicate a statistically significant increasing trend of about 0.005 mm d^{-1} yr^{-1} while GPCC gives an opposite trend of about –0.004 mm d^{-1} yr^{-1}; both trends are evaluated over the time period 1950–2009. GPCP gives a statistically significant decreasing trend of –0.010 mm d^{-1} yr^{-1} in the same region and season but computed on a shorter period of time (1979–2010). In the Himalaya during summer the CRU data indicate a decreasing precipitation trend (–0.008 mm d^{-1} yr^{-1}), which is not significant at the 95% confidence level (p=0.1). On the other hand, a statistically significant trend in summer precipitation in the Himalaya is provided by two out of the three longest observational data sets (APHRODITE and GPCC, covering almost the same period of time), corresponding to a decrease of about, respectively, –0.010 mm d^{-1} yr^{-1} (–0.57 mm d^{-1}(57 years)$^{-1}$), and –0.021 mm d^{-1} yr^{-1} (–1.25 mm d^{-1}(60 years)$^{-1}$). The analysis of the APHRODITE daily time series allows to explore whether the observed decreasing trend in total precipitation is associated with changes in the distribution of intense precipitation episodes. In Figure 10 we show the evolution of the amplitude distribution of daily precipitation from 1951 to 2007 in the Himalaya during summer, reporting the 99th, 95th, and 90th percentile lines (Figure 10a), the daily precipitation intensity (Figure 10b), the number of wet days during the warm season (defined as the number of days with precipitation greater than 1 mm d^{-1}, Figure 10c), and the evolution of the hydroclimatic intensity (HY-INT) index (Figure 10d), introduced by *Giorgi et al*. [2011]. This index is defined as the product of the average precipitation intensity in mm d^{-1} and the average dry spell length in days (here normalized to their values in the period 1951–2007). The analysis of the APHRODITE daily time series shows that the observed decrease in total precipitation corresponds to a statistically significant decreasing trend in precipitation intensity (–0.009 mm d^{-1} yr^{-1}, p=0.002).

[40] A statistically significant decreasing trend in monsoon and overall annual precipitation and an increasing but statistically insignificant trend in winter precipitation over the period 1866–2006 was found by *Bhutiyani et al*. [2010] for the northwestern Himalayan region. Other studies, such as the paper by *Shrestha et al*. [2000] which analyses precipitation data from Nepal over the past three decades, showed large interannual and decadal variability in the all-Nepal as well as regional (within Nepal)

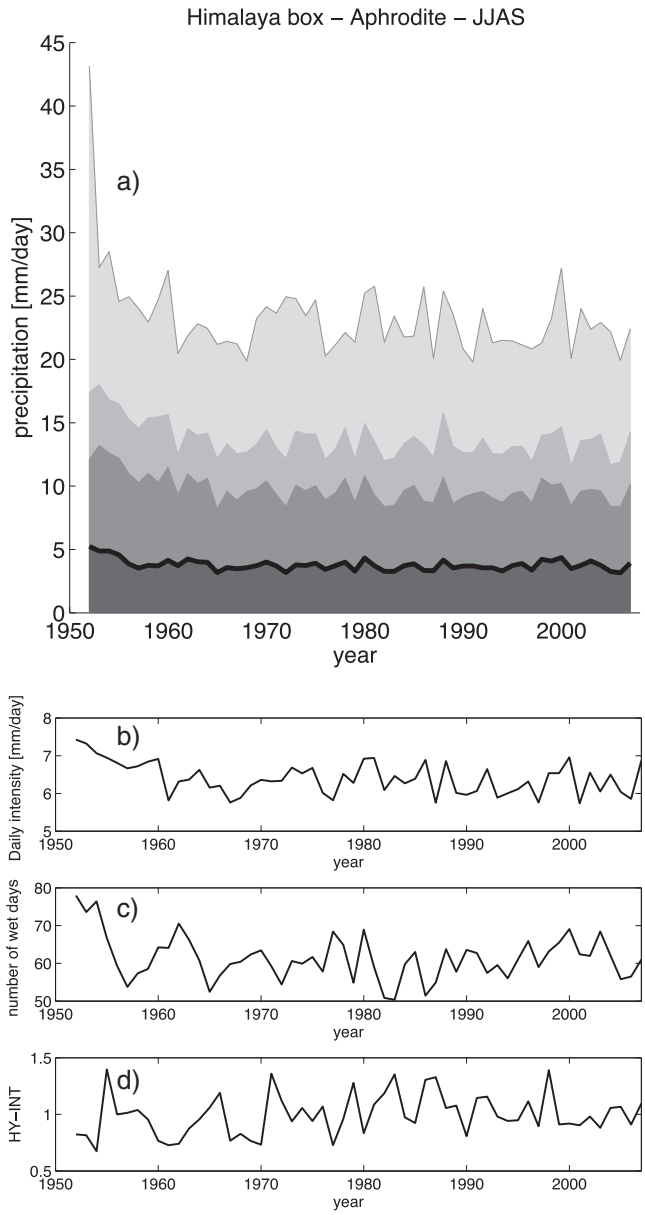

Figure 10. Precipitation statistics for APHRODITE in the Himalaya domain during summer. Time series of (a) average daily precipitation (black thick line) and precipitation above the 90th, 95th, and 99th percentiles (shaded regions); (b) daily precipitation intensity; (c) number of days with precipitation larger than 1 mm d^{-1} (wet days); and (d) the hydroclimatic index HY-INT.

precipitation records, but an absence of long-term trends in the precipitation records.

[41] Unlike the observations, EC-Earth indicates an increasing trend of monsoon precipitation in the Himalaya domain in the period 1950–2005. This could be due to the fact that the countering effects of the recent increases of atmospheric aerosol resulting from the combustion of fossil fuels in Asia [*Ramanathan et al*., 2005] is not correctly reproduced and/or to an improper representation of aerosols in this climate model. We will further discuss historical long-term variations in the EC-Earth model precipitation

output in the next section, along with the EC-Earth future precipitation trends under different emission scenarios.

4. Precipitation Scenarios in HKKH

[42] The EC-Earth model allows for analyzing projections of summer and winter precipitation in the HKK and Himalaya in the two emission scenarios RCP 4.5 and RCP 8.5 introduced in section 2. To this purpose, we extend the individual EC-Earth simulation discussed above and consider an ensemble of independent realizations created, under the same historical and future forcing conditions, by the participants in the EC-Earth consortium. These data, which allow for estimating natural climate variability in the EC-Earth modeling system, are publicly available on the "Climate Explorer" web site of KNMI (http://climexp.knmi.nl/). Figure 11 shows the time series of precipitation (after filtering with a 5 years running mean) from the resulting eight-member ensemble in the historical period (1850–2005) and for the future (2006–2100) in the RCP 4.5 scenario, for the two subregions of HKK (Figures 11a and 11b) and Himalaya (Figures 11c and 11d), averaged over winter (Figures 11a and 11c) and summer (Figures 11b and 11d). In order to highlight the interannual variability of the model precipitation, we report the EC-Earth simulation used above with a thick black line. Figure 12 shows the same as Figure 11, but for the more extreme RCP 8.5 scenario.

[43] As already noted in the previous section, Figures 11 and 12 show that in Himalaya during summer (Figures 11d and 12d), EC-Earth indicates an increasing trend of

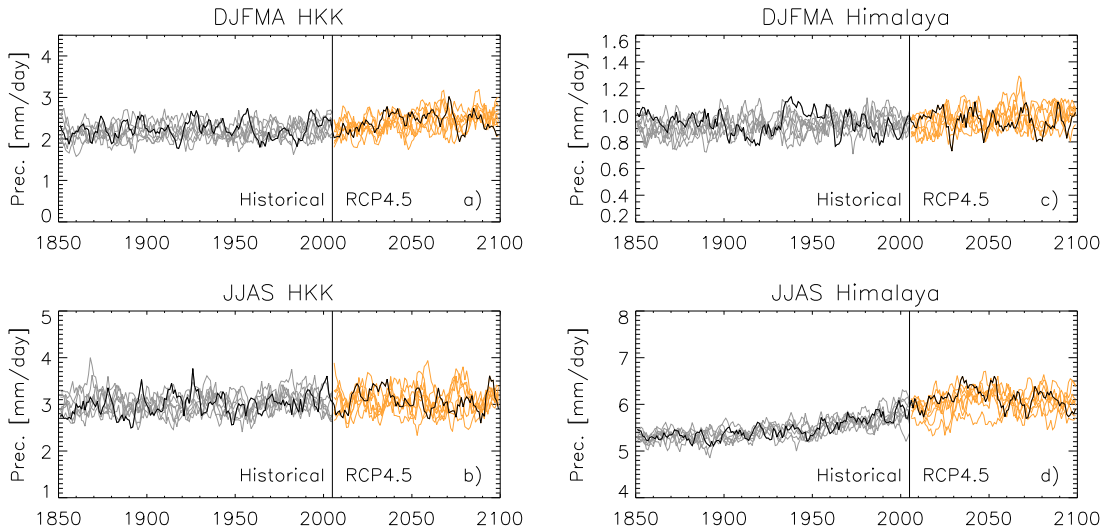

Figure 11. Time series of precipitation over (a and b) HKK and (c and d) the Himalaya domain during DJFMA (a and c) and JJAS (b and d) from the eight realizations of the EC-Earth model ensemble for the historical period (1850–2005, gray lines) and from 2006 to 2100 (orange lines) in the RCP 4.5 scenario. The individual member of the EC-Earth ensemble used in the previous analyses is indicated with a thick black line. The time series have been filtered with a 5 years running mean.

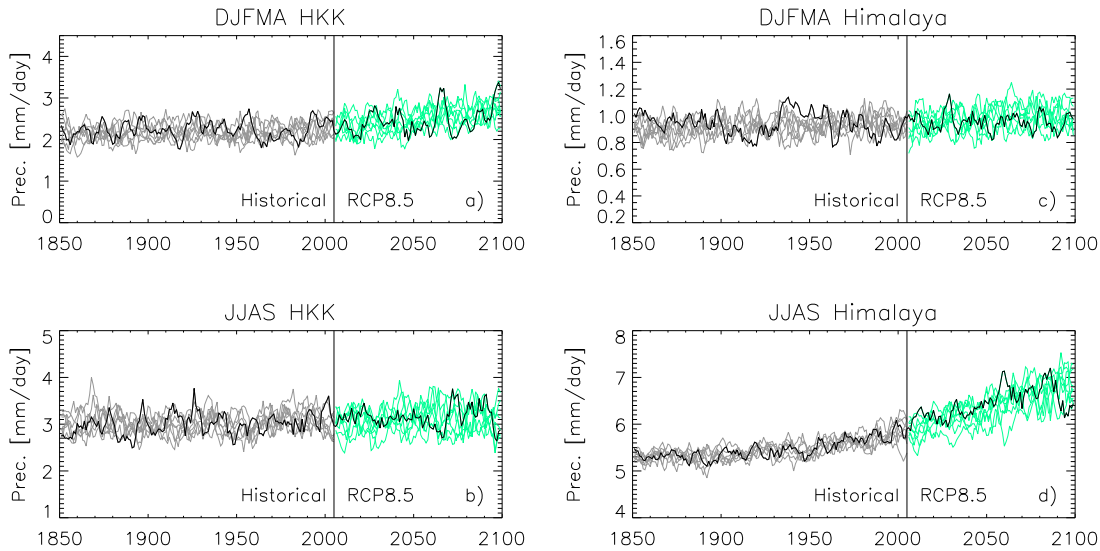

Figure 12. Same as Figure 11 but for the RCP 8.5 scenario.

precipitation in the period 1950–2009. Seven out of eight EC-Earth members actually give a statistically significant trend which corresponds to an increase in average precipitation rate between 0.005 and 0.010 mm d^{-1} yr^{-1}.

[44] The increasing trend in summer precipitation over the Himalaya is projected to continue under the most extreme RCP 8.5 scenario (Figure 12d). All eight EC-Earth members predict a statistically significant trend corresponding to an increase of about 0.008 to 0.014 mm d^{-1} yr^{-1} (average increase of about 0.8 to 1.2 mm d^{-1} in the period 2006–2100). In the RCP 4.5 scenario (Figure 11d), the increasing trend indicated by the model in the historical period continues till about 2050, when it stabilizes and a slight decrease starts. No statistically significant trend is found in the Himalaya in summer under the RCP 4.5 scenario. In the Himalaya during winter, one out of eight EC-Earth members provides a statistically significant increase in precipitation (0.08 mm d^{-1}(95 years)$^{-1}$) in the RCP 4.5 scenario, and another member shows a trend in future precipitation in the RCP 8.5 scenario corresponding to an increase of 0.16 mm d^{-1} (95 years)$^{-1}$.

[45] Three (five) out of eight EC-Earth members give a statistically significant increasing trend in winter precipitation in the HKK of about 0.3 to 0.4 (0.4 to 0.7) mm d^{-1}(95 years)$^{-1}$ under the RCP 4.5 (RCP 8.5) scenario. No statistically significant precipitation trend is found during summer in the HKK in the RCP 4.5 scenario, while in the RCP 8.5 scenario, two members give an increase in summer precipitation of about 0.5 mm d^{-1}(95 years)$^{-1}$.

[46] We further explore the trend in precipitation found for the Himalaya in summer in the two future scenarios. The analysis of daily time series shows that this trend is associated with changes in the distribution of intense precipitation episodes. In Figures 13a and 13e we report the evolution of the amplitude distribution of daily precipitation from 1850 to 2100 in the Himalaya during summer, reporting the 99th, 95th, and 90th percentile lines. For both scenarios, the increasing trend in summer precipitation over the Himalaya is associated with an increasing trend in precipitation extremes. For the RCP 8.5 scenario, in particular, daily precipitation intensity (Figure 13f) is projected to increase through the 21st century, in line with the increase in precipitation extremes (~1.3 mm d^{-1} over the period 2006–2100). The number of wet days during the warm season (Figure 13g) shows a significant decreasing trend (~8 days

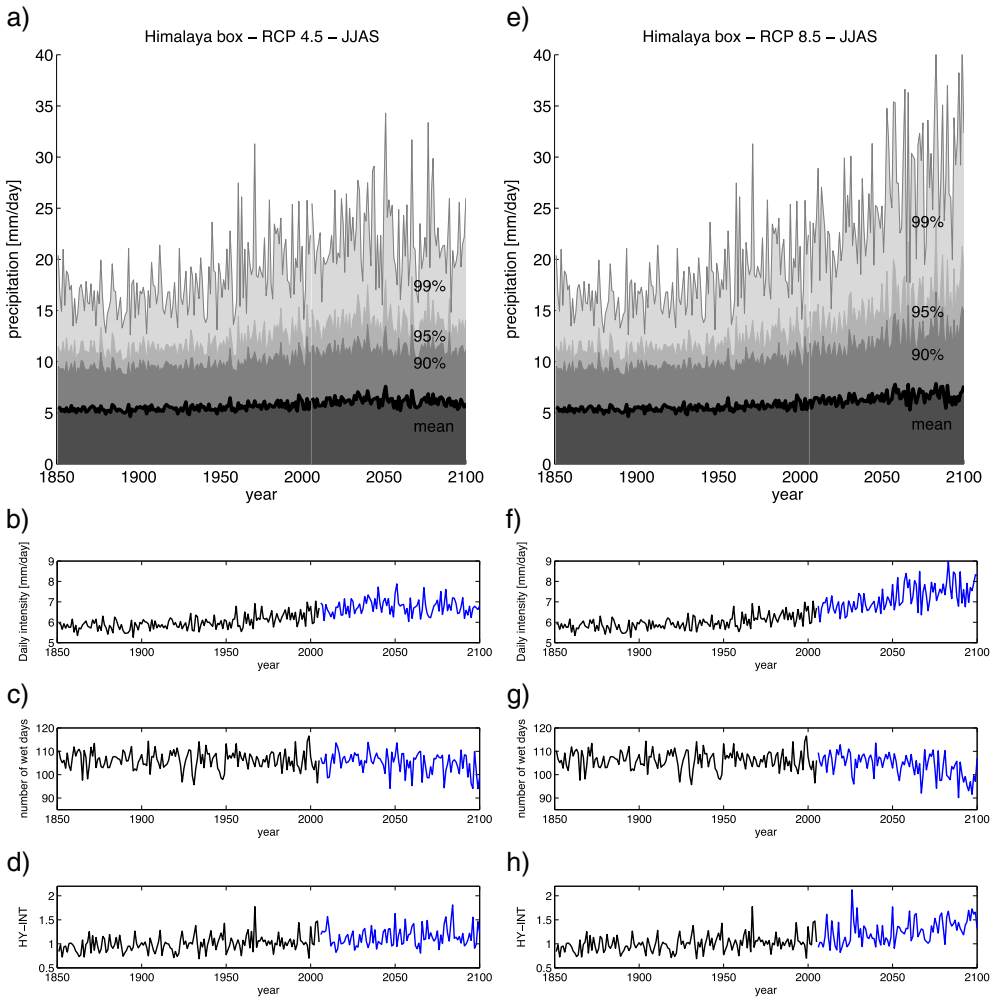

Figure 13. Precipitation statistics for EC-Earth. Time series of (a,e) average daily precipitation (black thick line) and precipitation above the 90th, 95th, and 99th percentiles (shaded regions); (b,f) daily precipitation intensity; (c,g) number of days with precipitation larger than 1 mm d^{-1} (wet days); and (d,h) the hydroclimatic index HY-INT, for the Himalaya domain during summer. (left) RCP 4.5; (right) RCP 8.5 scenario.

over 2006–2100). This is in line with climate projections at the global scale, which indicate for the 21st century an increase in precipitation intensity and number of dry days in response to increased greenhouse gas concentrations, although with pronounced regional variability [*Solomon et al*., 2007]. The RCP 4.5 scenario presents a similar picture, with an increase followed by stabilization of precipitation intensity at mid-21st century (Figure 13b). The number of wet days does present a weak, but significant trend (–4.5 days in 2006–2100, Figure 13c).

[47] We also discuss changes in hydroclimatic intensity computing the HY-INT index introduced by *Giorgi et al*. [2011]. As mentioned above, HY-INT is defined as the product of the average precipitation intensity in mm d^{-1} and the average dry spell length in days, here both normalized to their values in the period 1850–2005. The HY-INT index is sensitive to increases in both quantities which define it and has been found to be an ubiquitous signature, in several regions of the world, of 21st century global warming. The evolution of the index is reported in Figures 13d and 13h. We find a significant positive trend in HY-INT in the Himalaya for the RCP 8.5 scenario (0.38 in the period 2006–2100), indicating a trend toward more episodic and intense monsoonal precipitation. This result is consistent with the changes found for the number of dry days and precipitation intensity, in agreement with *Giorgi et al*. [2011] where an increase was found for the Indian region for different models in the A1B scenario. No significant trend in the 21st century can be found for HY-INT in the RCP 4.5 scenario simulated by EC-Earth. The projected increase of HY-INT in the RCP 8.5 scenario should however be taken with caution, both because no significant trend is visible in the more moderate RCP 4.5 scenario and because most climate models indicate an intensification of the hydrological cycle in the Himalaya during summer also in the last 50 years, which is not supported by the observations.

5. Discussion and Conclusions

[48] The complex meteoclimatic regimes in different parts of the HKKH range hamper a description of this area in terms of a homogeneous region and call for a division into subregions. In this work we have considered separately two main areas, the HKK in the west and the Himalaya in the east, which are exposed to different circulations and precipitation patterns. In these regions, we have specifically analyzed the properties of precipitation in mountain areas located above 1000 m above mean sea level, focusing on precipitation patterns, seasonality and trends as revealed by various existing gridded precipitation data sets, including a satellite data set (the TRMM 3B42 product), rain gauge based collections (APRHODITE, CRU, GPCC), a merged satellite and rain gauge climatology (GPCP), a reanalysis product (ERA-Interim), and precipitation data from a state-of-the-art GCM (EC-Earth).

[49] All the currently available gridded observational data sets are perforce limited to coarse resolutions. This makes them suitable for large-scale global studies, and for applications such as the comparison and validation of climate models at global scales or the comparison with global reanalysis products. Their application to assess the climate in smaller and orographically complex regions, such as the HKKH, is more difficult owing to their limited resolution and the limited coverage and inhomogeneities in the spatial and altitudinal distribution of the measuring sites. Our analysis shows that it is anyway possible to obtain a consistent picture of climate at the seasonal scale from these data sets in terms of area averages over subregions of the HKKH. On the other hand, there are severe difficulties in considering any of these observational/reanalysis data sets as a reference or ground truth for precipitation, and thus multiprobe source data should always be considered for estimating the hydrological cycle in these areas. Similar considerations can be applied to other regions: *Carvalho et al*. [2012], for instance, studied the South American monsoon system comparing several gridded precipitation data sets with different interpolation and gridding schemes, including the GPCP and TRMM 3B42 products also used in this study, and discussed the issues related to the use of such data sets.

[50] The mean annual cycle of precipitation over HKK and Himalaya is coherently reproduced by the various data sets. In the HKK it is characterized by a bimodal precipitation distribution, reflecting the wintertime precipitation associated with the western weather patterns and the impact of the summer monsoon. In the Himalaya, the dominant source of precipitation is the summer monsoon, leading to a unimodal precipitation distribution peaked around July. ERA-Interim strongly overestimates precipitation compared to the other data sets, and so does EC-Earth in the HKK domain, probably owing to the fact that both ERA-Interim and EC-Earth provide total precipitation while the in situ station and satellite data, as well as their combinations, have difficulties in detecting the snow component of precipitation. The analysis of liquid-only precipitation in ERA-Interim and EC-Earth generally gives results closer to the observations. However, EC-Earth liquid precipitation still keeps considerably lower than the total precipitation and lower than the observed precipitation, suggesting that the model may overestimate snowfall. This issue could be attributed to an existing cold bias in EC-Earth [*Hazeleger et al*., 2012].

[51] The precipitation time series from the various data sets in the time period 1950–2010 reproduce, in spite of the biases between the data sets, the interannual precipitation variability in a coherent way. None of the data sets shows statistically significant trends in the HKK during winter. In the Himalaya during summer, a statistically significant decreasing trend is observed from the analysis of the longest data sets (APHRODITE, CRU, and GPCC). Outputs from EC-Earth indicate a positive summer precipitation trend in this region, opposite to what is revealed by the observations: a possible explanation for the discrepancy between the decreasing trend in the observations and the increasing monsoon precipitation predicted by EC-Earth is that the model does not correctly reproduce the complex effect of the recent increase of atmospheric aerosols resulting from the combustion of fossil fuels in Asia [*Ramanathan et al*., 2005; *Lau et al*., 2006; *Bollasina et al*., 2011].

[52] Projections made with EC-Earth under two different emission scenarios, RCP 4.5 and RCP 8.5, show for RCP 4.5 that the historical increasing precipitation trend in the Himalaya during summer is predicted to continue until about 2050, starting a slight decrease from that time on. In the RCP 8.5 scenario, summer precipitation is found to increase throughout the century, associated with an increasing trend

in the intensity of rainfall events, a slight reduction of the number of rainy days. In this scenario, the hydroclimatic intensity index by *Giorgi et al*. [2011] is also found to increase, indicating a transition toward more episodic and intense monsoonal precipitation. Overall, these results agree with most current climate model projections [*Solomon et al*., 2007] giving an increase in wet extremes, in the length of dry periods and in precipitation in the Indian monsoon by the end of the 21st century, as a result of atmospheric moisture build-up due to increased greenhouse gases and consequent temperature increase. Future projections in the HKKH region should be further verified with climate models interactively resolving temporally varying radiative and thermodynamical effects of various aerosol species (however, this class of models is currently not included in the IPCC-CMIP5 ensemble).

[53] The data sets considered here did not confirm the view of an increasing winter precipitation trend in the Karakoram [*Archer and Fowler*, 2004], sometimes indicated as one of the possible causes of the snow cover increase and slight glacier advance in this area [*Tahir et al*., 2011; *Gardelle et al*., 2012], a well-known anomaly of Karakoram glaciers known since at least 30 years [*Hewitt*, 2005]. On the other hand, also the protecting effect on glacier melting of the debris cover, at least in the ablation areas of nonsurging glaciers between 3000 and 5000 m above mean sea level, has recently been questioned [*Gardelle et al*., 2012]. The high number of glacier surges [*Hewitt*, 2007; *Quincey et al*., 2011] in the region makes the situation and interpretation of the few available observations rather complex: the anomalous behavior of the Karakoram cryosphere still remains partly unexplained or, at least, not univocally understood.

[54] In this work, we did not explore the mechanisms associated with western weather patterns coming from the Mediterranean, which are responsible for winter precipitation in the western stretches of the HKKH, as well as their strengthening as they encounter a region of enhanced low pressure or their possible enrichment in terms of moisture from the Caspian Sea. These issues have been addressed in other studies, making use of both observations [*Syed et al*., 2006] and modeling approaches [*Syed et al*., 2010], and they are beyond the scope of this study. Similarly, we did not explore the issue of possible dynamical changes in the monsoon dynamics and in episodic intense precipitation events. This problem is of the utmost importance, as evidenced by the 2010 summer floods in Pakistan which were associated with anomalous patterns of the atmospheric circulation [*Houze et al*., 2011]. Understanding whether the probability of such events could change in the coming decades is a crucial issue to be explored in future studies. A resolution higher than that offered by the data sets employed in this work, both for observations and models, is needed when hydrological models are to be driven for small-scale basins or for assessing hydrometeorological extremes. In these cases, the problem could be addressed with high-resolution nonhydrostatic atmospheric models, as well as with stochastic downscaling techniques capable of generating ensembles of high-resolution, stochastic fields of climate variables from coarse resolution observed or modeled fields [*Rebora et al*., 2006].

[55] **Acknowledgments**. This work was funded by the Ev-K2-CNR SHARE-PAPRIKA-Karakoram project and by the NextData project of the Italian Ministry of Education, University and Research. The numerical simulations with the EC-Earth model used in this study were performed at the CASPUR supercomputing center, Rome, grant ext-06-EARTH. The ensemble of EC-Earth simulations analyzed in section 3 includes simulations created by other members of the EC-Earth consortium (http://ecearth.knmi.nl). These data are available as monthly averages on the "Climate Explorer" web site of KNMI (http://climexp.knmi.nl/) and from the official CMIP5 archives. We acknowledge the institutions and the teams responsible for the creation and publication of the GPCC, GPCP, APHRODITE, CRU, TRMM, and ERA-Interim archives. GPCP data provided by the NOAA/OAR/ESRL PSD, Boulder, CO, USA, from their Web site at http://www.esrl.noaa.gov/psd/. ERA-Interim data have been obtained from the ECMWF Data Server. We acknowledge the reviewers—two anonymous referees and Bodo Bookhagen—for their useful comments and suggestions on a previous version of the manuscript.

References

Adler, R. F., et al. (2003), The version 2 global precipitation climatology project (GPCP) monthly precipitation analysis (1979-present), *J. Hydrometeor.*, *4*, 1147–1167, doi:10.1175/1525-7541(2003)004<1147:TVGPCP>2.0.CO;2.

Andermann, C., S. Bonnet, and R. Gloaguen (2011), Evaluation of precipitation data sets along the Himalayan front, *Geochem. Geophys. Geosyst.*, *12*, Q07023, doi:10.1029/2011GC003513.

Archer, D. R. (2001), The climate and hydrology of northern Pakistan with respect to assessment of flood risk to hydropower schemes, Tech. rep., GTZ/WAPDA.

Archer, D. R., and H. J. Fowler (2004), Spatial and temporal variations in precipitation in the upper Indus basin, global teleconnections and hydrological implications, *Hydrol. Earth Syst. Sci.*, *8*, 47–61, doi:10.5194/hess-8-47-2004.

Archer, D. R., and H. J. Fowler (2006), Conflicting signals of climate change in the upper Indus basin, *J. Climate*, *19*, 4276–4293, doi:10.1175/JCLI3860.1.

Barros, A. P., M. Joshi, J. Putkonen, and D. W. Burbank (2000), A study of the 1999 monsoon rainfall in a mountainous region in central Nepal using TRMM products and rain gauge observations, *Geophys. Res. Lett.*, *27*, 3683–3686, doi:10.1029/2000GL011827.

Bengtsson, L., S. Hagemann, and K. I. Hodges (2004), Can climate trends be calculated from reanalysis data?, *J. Geophys. Res.*, *109*, D11111, doi:10.1029/2004JD004536.

Bhutiyani, M. R., V. S. Kale, and N. J. Pawar (2010), Climate change and the precipitation variations in the northwestern Himalaya: 1866–2006, *Int. J. Climatol.*, *30*(4), 535–548, doi:10.1002/joc.1920.

Bollasina, M. A., Y. Ming, and V. Ramaswamy (2011), Anthropogenic Aerosols and the weakening of the south Asian summer monsoon, *Science*, *334*(6055), 502–505, doi:10.1126/science.1204994.

Bonasoni, P., et al. (2010), Atmospheric brown clouds in the Himalayas: first two years of continuous observations at the Nepal-climate observatory at pyramid (5079 m), *Atmos. Chem. Phys.*, *10*, 7515–7531, doi:10.5194/acp-10-7515-2010.

Bookhagen, B., and D. Burbank (2006), Topography, relief, and TRMM-derived rainfall variations along the Himalaya, *Geophys. Res. Lett.*, *33*, L08405, doi:10.1029/2006GL026037.

Bookhagen, B., and M. R. Strecker (2008), Orographic barriers, high-resolution TRMM rainfall, and relief variations along the eastern Andes, *Geophys. Res. Lett.*, *35*, L06403, doi:10.1029/2007GL032011

Bookhagen, B., and D. Burbank (2010), Toward a complete Himalayan hydrological budget: Spatiotemporal distribution of snowmelt and rainfall and their impact on river discharge, *J. Geophys. Res.*, *115*, F03019, doi:10.1029/2009JF001426.

Carvalho, L. M. V., C. Jones, A. N. D. Posadas, R. Quiroz, B. Bookhagen, B. Liebmann (2012), Precipitation characteristics of the South American monsoon system derived from multiple datasets, *J. Climate*, *25*, 4600–4620, doi:10.1175/JCLI-D-11-00335.1.

Ciccarelli, N., J. von Hardenberg, A. Provenzale, C. Ronchi, A. Vargiu, and R. Pelosini (2008), Climate variability in north-western Italy during the second half of the 20th century, *Global Planet. Change*, *63*, 185–195, doi:10.1016/j.gloplacha.2008.03.006.

Dutra, E., G. Balsamo, P. Viterbo, P. M. A. Miranda, A. Beljaars, C. Schär, and K. Elder (2010), An improved snow scheme for the ECMWF land surface model: Description and offline validation, *J. Hydrometeor.*, *11* (4), 899–916, doi:10.1175/2010JHM1249.1.

Dutra, E., P. Viterbo, P. M. A. Miranda, and G. Balsamo (2011), Complexity of snow schemes in a climate model and its impact on surface energy and hydrology, *J. Hydrometeor.*, doi:10.1175/jhm-d-11-072.1.

Fichefet, T., and M. Morales-Maqueda (1997), Sensitivity of a global sea ice model to the treatment of ice thermodynamics and dynamics, *J. Geophys. Res.*, *102*, 12609–12646, doi:10.1029/97JC00480.

Gardelle, J., E. Berthier, and Y. Arnaud (2012), Slight mass gain of Karakoram glaciers in the early twenty-first century, *Nature Geosci.*, Online, doi:10.1038/NGEO1450.

Giorgi, F., E.-S. Im, E. Coppola, N. S. Diffenbaugh, X. J. Gao, L. Mariotti, and Y. Shi (2011), Higher hydroclimatic intensity with global warming, *J. Climate*, *24*, 5309–5324, doi:10.1175/2011JCLI3979.1.

Hazeleger, W., et al. (2012), EC-Earth v2.2: description and validation of a new seamless earth system prediction model, *Clim. Dynam.*, pp. 1–19, doi:10.1007/s00382-011-1228-5.

Hewitt, K. (2005), The Karakoram anomaly? glacier expansion and the 'elevation effect', Karakoram Himalaya, *Mt. Res. Dev.*, *25*, 332–340, doi:10.1659/0276-4741(2005)025[0332:TKAGEA]2.0.CO;2.

Hewitt, K. (2007), Tributary glacier surges: An exceptional concentration at Panmah Glacier, Karakoram Himalaya, *J. Glaciol.*, *53*, 181–188, doi:10.3189/172756507782202829.

Houze, R., K. Rasmussen, S. Medina, S. Brodzik, and U. Romatschke (2011), Anomalous atmospheric events leading to the summer 2010 floods in Pakistan, *BAMS*, *March Issue*, 291–298, doi:10.1175/2010BAMS3173.1.

Huffman, G. J., and et al., (2007), The TRMM Multisatellite Precipitation Analysis (TMPA): Quasi-global, multiyear, combined-sensor precipitation estimates at fine Scales. *J. Hydrometeor.*, *8*, 38–55, doi:10.1175/JHM560.1.

Kamal-Heikman, S., L. A. Derry, J. R. Stedinger, and C. C. Duncan (2007), A simple predictive tool for lower Brahmaputra river basin monsoon flooding. *Earth Interact.*, *11*, 1–11, doi:10.1175/EI226.1

Krishnamurti, T. N., and C. M. Kishtawal (2000), A pronounced continental-scale diurnal mode of the Asian summer monsoon, *Mon. Wea. Rev.*, *128*, 462–473.

Krishnamurti, T. N., A. K. Mishra, A. Simon, and A. Yatagai (2009), Use of a dense rain-gauge network over India for improving blended TRMM products and downscaled weather models, *J. Meteorol. Soc. Jpn.*, *87A*, 393–412, doi:10.2151/jmsj.87A.393.

Lau, K., M. Kim, and K. Kim (2006), Asian monsoon anomalies induced by aerosol direct forcing, *Clim. Dynam.*, *26*, 855–864, doi:10.1007/s00382-006-0114-z.

Li, C., and M. Yanali (1996), The onset and interannual variability of the Asian summer monsoon in relation to land–sea thermal contrast, *J. Climate*, *9*, 358–375, doi:10.1175/1520-0442(1996)009<0358:TOAIVO>2.0.CO;2.

Madec, G. (2008), NEMO ocean engine, Tech. rep., Note du Pole de modélisation 27, Institut Pierre- Simon Laplace (IPSL), France, ISSN No 1288-1619.

Mayer, C., A. Lambrecht, M. Belò, C. Smiraglia, and G. Diolaiuti (2006), Glaciological characteristics of the ablation zone of Baltoro glacier, Karakoram, Pakistan, *Ann. Glaciol.*, *43*, 123–131, doi:10.3189/172756406781812087.

Mitchell, T. D.,P. D. Jones (2005), An improved method of constructing a database of monthly climate observations and associated high-resolution grids, *Int. J. Climatol.*, *25*(6), 693–712, doi:10.1002/joc.1181.

Moss, R. H., et al. (2010), The next generation of scenarios for climate change research and assessment, *Nature*, *463*(7282), 747–756, doi:10.1038/nature08823.

New, M., M. Todd, M. Hulme, and P. Jones (2001), Precipitation measurements and trends in the twentieth century, *Int. J. Climatol.*, *21*(15), 1889–1922, doi:10.1002/joc.680.

Quincey, D. J., M. Braun, N. F. Glasser, M. P. Bishop, K. Hewitt, and A. Luckman (2011), Karakoram glacier surge dynamics, *Geophys. Res. Lett.*, *38*, L18504, doi:10.1029/2011GL049004.

Ramanathan, V., et al. (2005), Atmospheric brown clouds: Impacts on south Asian climate and hydrological cycle, *Proc. Natl. Acad. Sci.*, *102*, 5326–5333, doi:10.1073/pnas.0500656102.

Rasmussen, R., et al. (2012), How well are we measuring snow?, *BAMS*, *June 2012*, 811–829, doi:10.1175/BAMS-D-11-00052.1.

Rebora, N., L. Ferraris, J. von Hardenberg, and A. Provenzale (2006), RainFARM: Rainfall downscaling by a filtered autoregressive model, *J. Hydrometeor.*, *7*, 724–738, doi:10.1175/JHM517.1.

Riahi, K., S. Rao, V. Krey, C. Cho, V. Chirkov, G. Fischer, G. Kindermann, N. Nakicenovic, and P. Rafaj (2011), RCP 8.5–a scenario of comparatively high greenhouse gas emissions, *Clim. Chang.*, *109*, 33–57, doi:10.1007/s10584-011-0149-y.

Scherler, D., B. Bookhagen, and M. Strecker (2011), Spatially variable response of Himalayan glaciers to climate change affected by debris cover, *Nature Geosci.*, *4*, 156–159, doi:10.1038/ngeo1068.

Schmidt, S., and M. Nusser (2009), Fluctuations of Raikot glacier during the past 70 years: A case study from the Nanga Parbat massif, northern Pakistan, *J. Glaciol.*, *55*(194), 949–959, doi:10.3189/002214309790794878.

Shrestha, A. B., C. P. Wake, J. E. Dibb, and P. A. Mayewski (2000), Precipitation fluctuations in the Nepal Himalaya and its vicinity and relationship with some large scale climatological parameters, *Int. J. Climatol.*, *20*(3), 317–327, doi:10.1002/(SICI)1097-0088(20000315)20:3<317::AID-JOC476>3.0.CO;2-G.

Singh, P., K. S. Ramashastri, and N. Kumar (1995), Topographic influences on precipitation distribution in different ranges of the western Himalayas, *Nord. Hydrol.*, *26*, 259–284, doi:10.2166/nh.1995.015.

Sohn, S.-J., C.-Y. Tam, K. Ashok, and J. Ahn (2011), Quantifying the reliability of precipitation datasets for monitoring large-scale east Asian precipitation variations, *Int. J. Climatol.*, doi:10.1002/joc.2380.

Solomon, S., D. Qin, M. Manning, M. Marquis, K. B. Averyt, M. Tignor, H. L. Miller, and Z. Chen (2007), Climate Change 2007: The physical science basis. contribution of working group I to the fourth assessment report of the Intergovernmental Panel on Climate Change.

Syed, F. S., F. Giorgi, J. S. Pal, and M. P. King (2006), Effect of remote forcings on the winter precipitation of central southwest Asia part 1: observations, *Theor. Appl. Climatol.*, *86*(1–4), 147–160, doi:10.1007/s00704-005-0217-1.

Syed, F. S., F. Giorgi, J. S. Pal, and K. Keay (2010), Regional climate model simulation of winter climate over CentralSouthwest Asia, with emphasis on NAO and ENSO effects, *Int. J. Climatol.*, *30*(2), 220–235, doi:10.1002/joc.1887.

Tahir, A., P. Chevallier, Y. Arnaud, and B. Ahmad (2011), Snow cover dynamics and hydrological regime of the Hunza river basin, Karakoram range, northern Pakistan, *Hydrol. Earth Sys. Sci.*, *15*, 2275–2290, doi:10.5194/hess-15-2275-2011.

Thomson, A. M., et al. (2011), RCP4.5: a pathway for stabilization of radiative forcing by 2100, *Clim. Chang.*, doi:10.1007/s10584-011-0151-4.

Treydte, K. S., G. H. Schleser, G. Hrllr, D. C. Frank, W. Winiger, G. H. Haug, and J. Esper (2006), The twentieth century was the wettest period in northern Pakistan over the past millennium, *Nature*, *440*, 1179–1182, doi:10.1038/nature04743.

Winiger, M., M. Gumpert, and H. Yamout (2005), Karakorum-Hindukush-western Himalaya: assessing high altitude water resources., *Hydrol. Process.*, *19*, 2329–2338, doi:10.1002/hyp.5887.

Wu, G., and Y. Zhang (1998), Tibetan plateau forcing and the timing of the monsoon onset over south Asia and the south China sea, *Mon. Wea. Rev.*, *126*, 913–927, doi:10.1175/1520-0493.

Yatagai, A., and H. Kawamoto (2009), Quantitative estimation of orographic precipitation over the Himalayas by using TRMM/pr and a dense network of rain gauges, in *Proc. of SPIE*, vol. *7148*, doi:10.1117/12.811943.

Yatagai, A., O. Arakawa, K. Kamiguchi, H. Kawamoto, M. I. Nodzu, and A. Hamada (2009), A 44-year daily gridded precipitation dataset for Asia based on a dense network of rain gauges, *SOLA*, *5*, 137–140, doi:10.2151/sola.2009-035.

Yatagai, A., K. Kamiguchi, O. Arakawa, A. Hamada, N. Yasutomi, and A. Kitoh (2012), APHRODITE: Constructing a long-term daily gridded precipitation dataset for Asia based on a dense network of rain gauges, *Bull. Amer. Meteor. Soc.*, *93*, 1401–1415, doi:10.1175/BAMS-D-11-00122.1.